The Oncologist®

Neuro-Oncology

Comprehensive Genomic Profiling of 282 Pediatric Low- and High-Grade Gliomas Reveals Genomic Drivers, Tumor Mutational Burden, and Hypermutation Signatures

Adrienne Johnson,[a] Eric Severson,[a] Laurie Gay,[a] Jo-Anne Vergilio,[a] Julia Elvin,[a] James Suh,[a] Sugganth Daniel,[a] Mandy Covert,[a] Garrett M. Frampton,[a] Sigmund Hsu,[b] Glenn J. Lesser,[c] Kimberly Stogner-Underwood,[c] Ryan T. Mott,[c] Sarah Z. Rush,[d] Jennifer J. Stanke,[d] Sonika Dahiya,[e] James Sun,[a] Prasanth Reddy,[a] Zachary R. Chalmers,[a] Rachel Erlich,[a] Yakov Chudnovsky,[a] David Fabrizio,[a] Alexa B. Schrock,[a] Siraj Ali,[a] Vincent Miller,[a] Philip J. Stephens,[a] Jeffrey Ross,[a] John R. Crawford,[f] Shakti H. Ramkissoon[a]

[a]Foundation Medicine, Inc., Morrisville, North Carolina and Cambridge, Massachusetts, USA; [b]Department of Neurosurgery, University of Texas Health Science Center, Houston, Texas, USA; [c]Wake Forest Baptist Comprehensive Cancer Center, Winston-Salem, North Carolina, USA; [d]Department of Pediatrics, Division of Hematology and Oncology, Children's Hospital Medical Center of Akron, Akron, Ohio, USA; [e]Department of Pathology and Immunology, Washington University School of Medicine, St. Louis, Missouri, USA; [f]Department of Neurosciences and Pediatrics, University of California San Diego, San Diego, California, USA

Disclosures of potential conflicts of interest may be found at the end of this article.

Key Words. Pediatric neuro-oncology • Glioma • Precision medicine • Immunotherapy • Clinical sequencing

Abstract

Background. Pediatric brain tumors are the leading cause of death for children with cancer in the U.S. Incorporating next-generation sequencing data for both pediatric low-grade (pLGGs) and high-grade gliomas (pHGGs) can inform diagnostic, prognostic, and therapeutic decision-making.

Materials and Methods. We performed comprehensive genomic profiling on 282 pediatric gliomas (157 pHGGs, 125 pLGGs), sequencing 315 cancer-related genes and calculating the tumor mutational burden (TMB; mutations per megabase [Mb]).

Results. In pLGGs, we detected genomic alterations (GA) in 95.2% (119/125) of tumors. *BRAF* was most frequently altered (48%; 60/125), and *FGFR1* missense (17.6%; 22/125), *NF1* loss of function (8.8%; 11/125), and *TP53* (5.6%; 7/125) mutations were also detected. Rearrangements were identified in 35% of pLGGs, including *KIAA1549-BRAF*, *QKI-RAF1*, *FGFR3-TACC3*, *CEP85L-ROS1*, and *GOPC-ROS1* fusions. Among pHGGs, GA were identified in 96.8% (152/157). The genes most frequently mutated were *TP53* (49%; 77/157), *H3F3A* (37.6%; 59/157), *ATRX* (24.2%; 38/157), *NF1* (22.2%; 35/157), and *PDGFRA* (21.7%; 34/157). Interestingly, most *H3F3A* mutations (81.4%; 35/43) were the variant K28M. Midline tumor analysis revealed *H3F3A* mutations (40%; 40/100) consisted solely of the K28M variant. Pediatric high-grade gliomas harbored oncogenic *EML4-ALK*, *DGKB-ETV1*, *ATG7-RAF1*, and *EWSR1-PATZ1* fusions. Six percent (9/157) of pHGGs were hypermutated (TMB >20 mutations per Mb; range 43–581 mutations per Mb), harboring mutations deleterious for DNA repair in *MSH6, MSH2, MLH1, PMS2, POLE*, and *POLD1* genes (78% of cases).

Conclusion. Comprehensive genomic profiling of pediatric gliomas provides objective data that promote diagnostic accuracy and enhance clinical decision-making. Additionally, TMB could be a biomarker to identify pediatric glioblastoma (GBM) patients who may benefit from immunotherapy. ***The Oncologist*** 2017;22:1478–1490

Implications for Practice: By providing objective data to support diagnostic, prognostic, and therapeutic decision-making, comprehensive genomic profiling is necessary for advancing care for pediatric neuro-oncology patients. This article presents the largest cohort of pediatric low- and high-grade gliomas profiled by next-generation sequencing. Reportable alterations were detected in 95% of patients, including diagnostically relevant lesions as well as novel oncogenic fusions and mutations. Additionally, tumor mutational burden (TMB) is reported, which identifies a subpopulation of hypermutated glioblastomas that harbor deleterious mutations in DNA repair genes. This provides support for TMB as a potential biomarker to identify patients who may preferentially benefit from immune checkpoint inhibitors.

Correspondence: Shakti H. Ramkissoon, M.D., Ph.D., M.M.Sc., Foundation Medicine, Inc., 7010 Kit Creek Road, Morrisville, North Carolina 27560, USA. Telephone: 617-418-2200; e-mail: sramkissoon@foundationmedicine.com Received May 23, 2017; accepted for publication July 27, 2017; published Online First on September 14, 2017. http://dx.doi.org/10.1634/theoncologist.2017-0242

Introduction

Pediatric gliomas represent a diverse group of tumors of varying histologies, grades, and genetics. Broadly, these tumors can be divided into two major categories: pediatric low-grade (pLGG) and high-grade (pHGG) gliomas. Traditionally, gliomas have been diagnosed solely on histologic criteria; however, because morphologic overlap occurs frequently, there remains a need for objective data to promote diagnostic accuracy and support prognostic and therapeutic decision-making. With pediatric brain tumors surpassing leukemia as the leading cause of cancer-associated mortality among children, the need to identify new therapeutic strategies has never been greater [1].

The emergence of next-generation sequencing has helped identify key biomarkers, which in several instances are disease-defining alterations. Among pLGGs, *BRAF* alterations are most commonly observed in pilocytic astrocytomas, pleomorphic xanthoastrocytomas (PXA), gangliogliomas, and other glioneuronal lineage tumors [2–5]. Additionally, *MYB* alterations define subsets of pediatric diffuse gliomas, including *MYB-QKI* fusions for pediatric angiocentric gliomas [6, 7]. Mutations in histone proteins (*H3F3A*) reveal the importance and specificity of epigenome alterations in pHGGs [8–10].

Recently, checkpoint inhibitors (programmed death-ligand 1 [PD-L1] or programmed cell death protein 1 [PD-1] inhibitors) have emerged as potential therapeutic options for adult and pediatric high-grade gliomas [11–13]. Monoclonal antibodies that block PD-1 (pembrolizumab, nivolumab) or PD-L1 (atezolizumab) can boost the immune response against cancer cells and have shown promise in treating multiple cancer types [14]. Tumor mutational burden (TMB), defined as mutations per megabase (Mb), has proven to be a reliable biomarker for stratifying tumors (e.g., non-small cell lung cancer [NSCLC], melanoma) and is thought to serve as a proxy for overall neoantigen burden [15, 16]. The value of TMB as an objective biomarker in the setting of pediatric gliomas remains largely unexplored; however, there is increasing optimism that high TMB may be a biomarker to define a subset of pHGGs most likely to respond to checkpoint inhibitors [11, 17].

In this study, we highlight the value of comprehensive genomic profiling (CGP) in the largest known cohort of pediatric gliomas and explore the most common alterations across diagnosis and anatomic location. Additionally, we explore TMB and associated genetic factors that may predispose patients to developing a hypermutator phenotype.

Materials and Methods

Approval for this study, including a waiver of informed consent and a Health Insurance Portability and Accountability Act of 1996 waiver of authorization, was obtained from the Western Institutional Review Board (IRB number 20152817). Comprehensive genomic profiling was performed in a Clinical Laboratory Improvement Amendments-certified, College of American Pathologists-accredited, New York State-regulated reference laboratory (Foundation Medicine, Inc.). All samples underwent central histopathologic review by a board-certified neuropathologist (S.H.R.) using World Health Organization (WHO) criteria. At least 50 ng of DNA per specimen was extracted from 282 clinical formalin-fixed paraffin-embedded tumor samples, and next-generation sequencing was performed on hybridization-captured, adaptor ligation-based libraries to high, uniform coverage (>500 read coverage depth) for all coding exons of 315 cancer-related genes and 28 genes commonly rearranged in cancer (FoundationOne, Foundation Medicine Inc., Cambridge, MA, https://www.foundationmedicine.com; supplemental online Table 1). Sequence data were analyzed for clinically relevant classes of genomic alterations, including base pair substitutions, insertions/deletions, copy number alterations, and rearrangements/fusions. All gene amplification events reported in this study represent high-level amplification. Although we recognize that there are differences for naming *H3F3A* mutations in the literature, in this study, *H3F3A* variants (*H3F3A* K28M or G35R/V) align with current Catalogue of Somatic Mutations in Cancer nomenclature, but are equivalent to K27M or G34R/V [18]. Tumor mutational burden was calculated over 1.1 Mb as the number of somatic, coding point mutations and indels per Mb of genome (low: 0–<6; intermediate: 6–19; high: ≥20 mutations per Mb).

Results

Cohort Demographics

Comprehensive genomic profiling was performed on a cohort of 282 samples from pediatric patients diagnosed with low- and high-grade gliomas. The median age was 11 years and ranged from <1 to 18 years. Of the 282 patients, 50% (141/282) were male and 50% (141/282) were female (supplemental online Table 2). Tumors with noncategorical features were classified as low-grade glioma (LGG) not otherwise specified (NOS) or high-grade glioma (HGG) NOS. Integrated genomic analyses were then performed separately for pediatric HGGs (pHGGs) and LGGs (pLGGs). The pLGG cohort consisted of 125 patients (58 males and 67 females) with a median age of 9 years and ranging from <1 to 18 years, and included a diverse range of tumor types (supplemental online Table 3A). The mean tumor purity of samples was 30% and the mean coverage was 665X. The pHGGs consisted of 157 specimens of varying diagnoses (supplemental Table 3B) with a median age of 11 years (range: <1–18 years) and consisted of 83 males and 74 females. The mean tumor purity of samples was 65% and the mean coverage was 705X.

Genomic Landscape of pLGGs

Genomic alterations were identified in 95.2% (119/125) of pLGG specimens, with an average of 1.8 genomic alterations per specimen (Fig. 1A, 1B). *BRAF* was the most commonly altered gene, with variants detected in 48.0% (60/125) of cases including 26 base substitutions and 35 gene fusions. Other frequently altered genes included *FGFR1, NF1*, and *TP53*, which were reported in 17.6% (22/125), 8.8% (11/125), and 5.6% (7/125) of cases, respectively.

Among 46 pilocytic astrocytomas (PAs), 61% ($n = 28$) harbored *KIAA1549-BRAF* fusions, whereas 13% ($n = 6$) tumors harbored *BRAF* V600E mutations (supplemental online Fig. 1A). Interestingly, co-occurring alterations were detected in seven *KIAA1549-BRAF* PAs, including four with mutations in *TP53, ARID1A, MDM4*, or *BRCA1*, and three with *CDKN2A/B* deletions, and *CDK4* or *CDK6* amplifications. Of the 12 PAs in which *BRAF* alterations were not detected, 7 harbored *FGFR1*

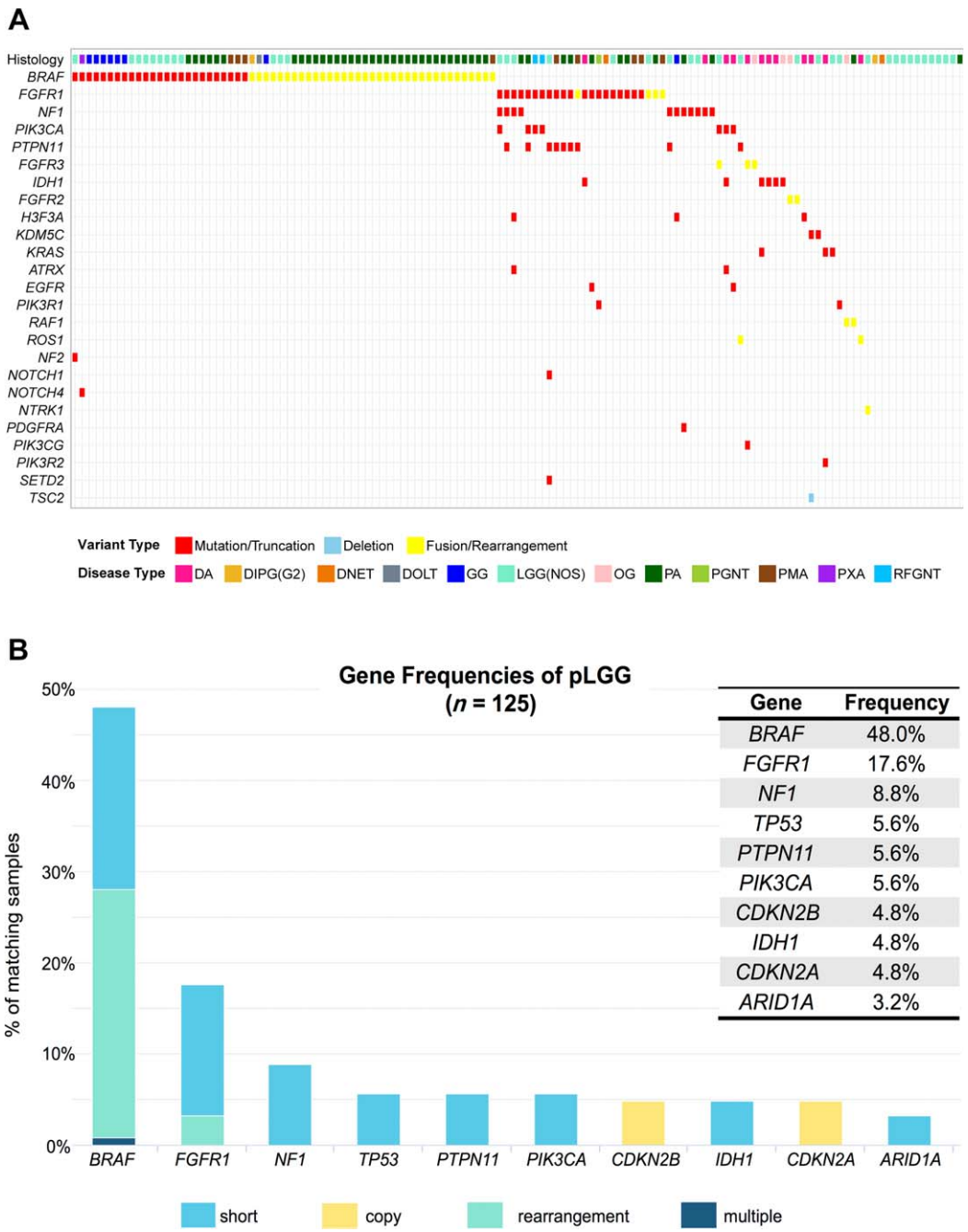

Figure 1. Genomic landscape of pLGGs. **(A)**: Tile plot illustrating the type of recurrent genomic alterations ($n \geq 2$) and corresponding histologic diagnosis in 125 pLGGs. **(B)**: Long-tail distribution highlighting the top 10 altered genes in the pLGG cohort. Types of alterations are color-coded using key at bottom of bar graph.

Abbreviations: DA, diffuse astrocytoma; DIPG(G2), diffuse intrinsic pontine glioma (grade II); DNET, dysembryoplastic neuroepithelial tumor; DOLT, disseminated oligodendroglial-like leptomeningeal tumor; GG, ganglioglioma; LGG, low-grade glioma; NOS, not otherwise specified; OG, oligodendroglial; PA, pilocytic astrocytoma; PGNT, papillary glioneuronal tumor; PMA, pilomyxoid astrocytoma; pLGG, pediatric low-grade glioma; PXA, pleomorphic xanthoastrocytomas; RFGNT, rosette forming glioneuronal tumor.

alterations, including 1 with a duplication, three *FGFR1* N546K, and three *FGFR1* K656E variants (supplemental online Fig. 1A). The correlation between anatomic location and *BRAF* or *FGFR1* alterations is illustrated in supplemental online Table 4. Five PAs without *BRAF* or *FGFR1* alterations had mutations in other pediatric glioma-associated genes. One tumor harbored a previously reported *QKI-RAF1* fusion co-occurring with a *NOTCH1* V1575I mutation, whereas an uncharacterized *EGFR* R222C extracellular domain mutation was the only alteration detected in another PA [7]. *NF1* loss-of-function mutations were detected in two PAs, with one tumor reporting a co-occurring *PDGFRA* A491T mutation. One other PA harbored *GLI1* P535S and *XRCC2* R258H mutations.

Of the 12 diffuse astrocytomas, *IDH1* and *TP53* mutations were the most frequent alterations, co-occurring in 41.6% (5/12) of cases (supplemental online Fig. 1B). These five *IDH1*-mutated tumors were from mid-to-late adolescence (ages 15–17) patients with genetics similar to adult diffuse astrocytomas,

which frequently harbor co-occurring *TP53* and *IDH1* mutations [19, 20]. Three of these *TP53/IDH1*-mutated tumors also harbored other mutations, including one tumor with *PIK3CA* D350H, *ACVR1B*, and *ATRX* frameshift mutations, another tumor with a *KRAS* G13D, and the third tumor with *FGFR1* K656E and *ALK* R1212H mutations. Of the seven DA2s without *IDH1* and *TP53* lesions, we detected an *FGFR3-TACC3* fusion co-occurring with a *PIK3CG* D238N mutation in one tumor and another tumor with a *CEP85L-ROS1* fusion (supplemental online Fig. 1B). Other tumors harbored *KRAS* Q61H and *PIK3R2* Q494* mutations, a *KDM5C* R179H mutation co-occurring with homozygous *TSC2* deletion, *NF1* frameshift mutations, or *EGFR* A289V and *PIK3CA* H1047R mutations. Furthermore, our cohort included a hypothalamic DA2 with an *H3F3A* K28M mutation, which raises the possibility that the tumor may follow a more aggressive clinical course as supported by recent studies. These showed that *H3F3A* K28M mutations are a negative prognostic factor among midline pLGGs. Additionally, in light of this finding, midline infiltrating LGGs harboring *H3F3A* K28M mutations may be best classified as the newly recognized entity, diffuse midline glioma *H3F3A*-K28M mutant (WHO grade IV) [10, 21, 22].

Glioneuronal tumors including gangliogliomas ($n = 8$), two rosette forming glioneuronal tumor (RFGNT) and one PXA, were enriched for *BRAF* alterations, specifically *BRAF* V600E mutations, which occurred in 63.6% (7/11) of cases (supplemental online Fig. 1C). In two cases, one GG and the PXA, the *BRAF* V600E mutation co-occurred with *CDKN2A/B* deletions. Interestingly, another ganglioglioma (GG) harbored a *TMEM106B-BRAF* fusion as well as loss of *CDKN2A/B*. We also identified a GG with an *H3F3A* K28M mutation co-occurring with an *APC* I307K and *NF1* frameshift mutations. Both RFGNTs harbored *PIK3CA* H1047R mutations, with one tumor harboring co-occurring *FGFR1* N546K and *BRIP1* A453T mutations (supplemental online Fig. 1C).

Among pLGG NOS tumors, the most common alterations involved *BRAF, FGFR*, and *NF1*, which occurred in 31.6% (12/38), 21.1% (8/38), and 15.8% (6/38) of cases, respectively (supplemental online Fig. 1D). Of the 12 cases with *BRAF* lesions, 7 harbored *BRAF* V600E mutations, with 5 tumors harboring co-occurring mutations including *CDKN2A/B* deletions, *RUNX1* deletion, *KEL* amplification, *ARID1A* Q1835* or *PRKDC* H1613R mutations. We also detected *KIAA1549-BRAF* fusions in three pLGG NOS tumors. Two other tumors harbored a *BRAF* G466V mutation or T599_V600 insertion. *FGFR* altered tumors ($n = 8$) included an *FGFR3-TACC3* fusion with a co-occurring *PIK3CA* M1043V mutation, *FGFR2-INA* fusion, and another tumor with an *FGFR1* duplication (supplemental online Fig. 1D). The other five tumors reported *FGFR1* point mutations, including two with *FGFR1* K656E variants and three with *FGFR1* N546K variants; four of these tumors harbored co-occurring mutations including *PIK3CA, NF1, or PTPN11* mutations. Of the six *NF1* mutated pLGG NOS tumors, three harbored co-occurring *FGFR1* mutations, and the other three tumors harbored co-occurring *MLL3*, *PTPN11*, or *ARID1A* and *CCND2* mutations.

Nine LGG NOS tumors harbored alterations in a variety of other glioma-associated genes. For example, in one tumor, we identified a *TPM3-NTRK1* fusion co-occurring with *CDKN2A/B* deletions. Another tumor harbored a *GOPC-ROS1* fusion with *TP53* and PTPN11 mutations. In the other seven tumors, we detected *DNMT3A* and *KDM5C*, *PIK3R1*, *BRCA2*, *KRAS*, *SLIT2*, *VHL*, or *ATM* and *CTNNB1* mutations. Taken together, these findings highlight a subset of LGG NOS tumors, which are difficult to classify solely on histologic features, but can be categorized by their genomic signatures for use in refining pathologic diagnoses and supporting clinical decision-making.

Of the nine PMAs in our cohort, five harbored *FGFR1* alterations, including three with K656E mutations and two with duplications. The other four PMAs harbored *BRAF* alterations wherein three tumors were V600E positive and the other had a *KIAA1549-BRAF* fusion co-occurring with *EPHB1* V322I mutation.

The less prevalent histologic subtypes included four oligodendrogliomas grade 2 (G2), two dysembryoplastic neuroepithelial tumour (DNET), two RFGNTs and one of each diffuse intrinsic pontine glioma (grade II) (DIPG G2), papillary glioneuronal tumor (PGNT), PXA (G2) and disseminated oligodendroglial-like leptomeningeal tumor (DOLT) (Fig. 2). Three of the four oligodendrogliomas harbored fusions including a *QKI-RAF1, FGFR2-PASD1*, or *FGFR3-TACC3*. The fourth tumor harbored *IDH1* R132H and *CIC* p1502fs*12 mutations, which is genomically similar to adult oligodendrogliomas [19]. In the two DNETs, a *DNMT3A* splice site mutation was detected in one tumor and an *FGFR1* K656E mutation with *SOX2* amplification in the other. Both RFGNTs harbored *PIK3CA* H1047R mutations, with one of the tumors reporting co-occurring *FGFR1* N546K and *BRIP1* A453T mutations. In the DIPG (G2), PGNT, PXA (G2), and DOLT a *KIAA1549-BRAF* fusion, *FGFR1* N546K and *PIK3R1* F456_Q457del, *BRAF* V600E, *CDKN2A/B* deletions, or *KIAA1549-BRAF* and *SMAD4* P295I alterations, were identified, respectively (Fig. 2).

With growing evidence for the role of targeted therapies in pediatric neuro-oncology, the value of CGP is eminently clear. In the case of an 11-year-old male diagnosed with neurofibromatosis type 1 and a cerebellar PA, multiply recurrent and treated with surgery alone, CGP identified *NF1* (splice site 2251 + 1G>A, splice site 3708 + 1G>A) and *PDGFRA* A491T alterations. Subsequent combination therapy with everolimus (mTOR inhibitor) and trametinib (MEK inhibitor) yielded a robust antitumor response. As demonstrated by T1 post-gadolinium coronal magnetic resonance imaging images (Fig. 2H), 3 months of dual inhibitor therapy resulted in a marked decrease in the enhancing component of this patient's tumor.

Genomic Landscape of pHGGs

We detected genomic alterations in 96.8% (152/157) of HGG specimens, with an average of 6.5 genomic alterations per sample (Fig. 3A, 3B). The most frequently mutated gene in this cohort was *TP53,* which was altered in 49% (77/157) of samples. Other frequently altered genes included *H3F3A* mutations in 37.6% (59/157), *NF1* loss of function mutations in 24.2% (38/157), *ATRX* loss of function mutations in 22.2% (35/157), and *PDGFRA* alterations in 21.7% (34/157) of pHGGs (Fig. 3A, 3B).

In our cohort of 90 GBMs, *TP53* was mutated in 62.2% (56/90) of cases, and *H3F3A* alterations were detected in 47.8% (43/90) of cases (Fig. 4A). Interestingly, the vast majority (81.4%, 35/43) of *H3F3A* mutations were the K28M variant, compared with 18.6% (8/43) being G35R variants. Although frequent in pLGGs, only five pediatric glioblastoma (pGBM)s harbored *BRAF* V600E mutations, and of these tumors, four harbored co-occurring *H3F3A* K28M mutations. Unlike adult

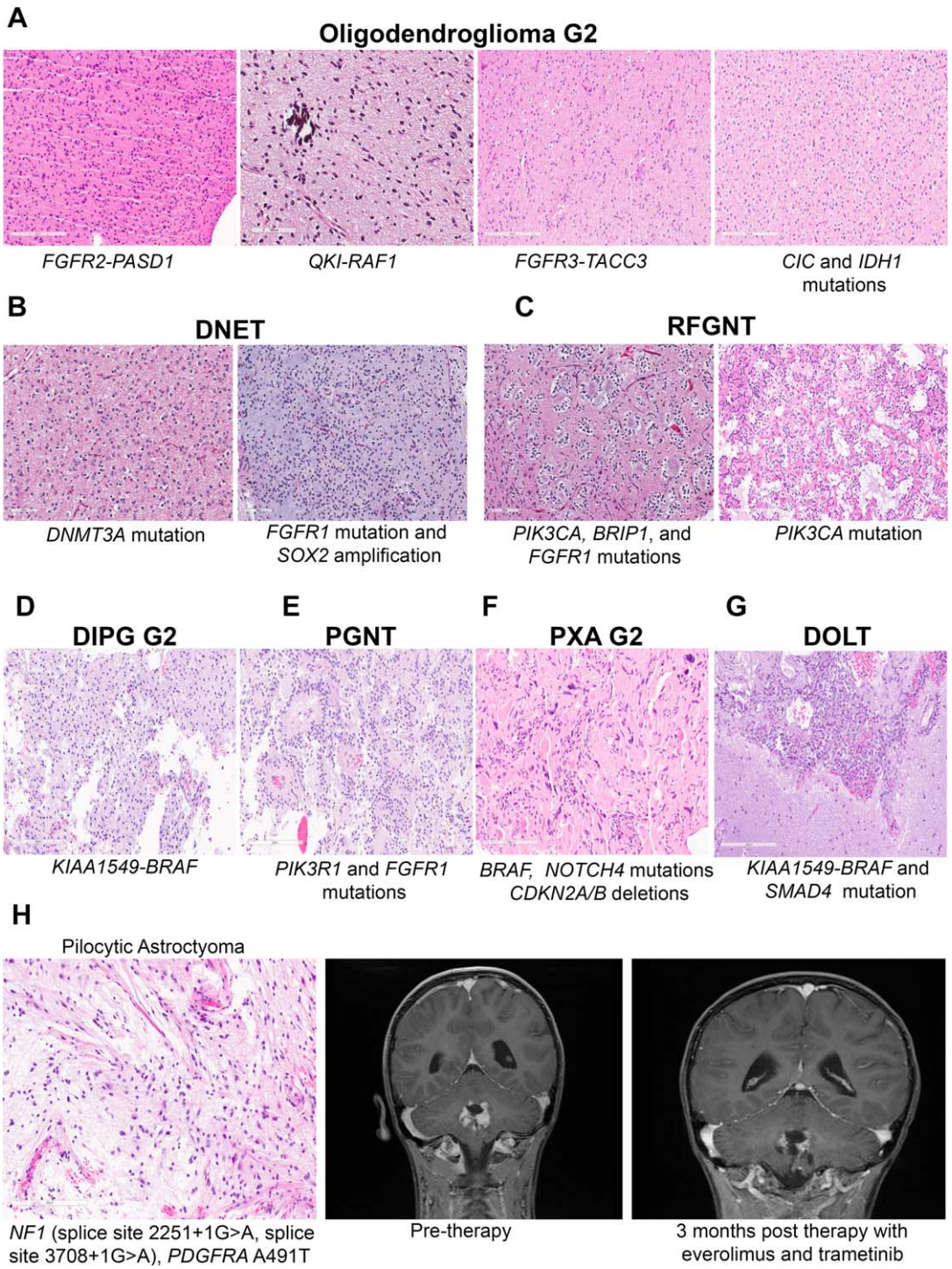

Figure 2. Histologic subtypes and associated genomic alterations. Hematoxylin and eosin (H&E) staining and corresponding genomic alteration for four oligodendrogliomas **(A)**, two DNETs **(B)**, two RFGNTs **(C)**, one DIPG G2 **(D)**, one PGNT **(E)**, one PXA G2 **(F)**, and one DOLT **(G)**. **(H)**: H&E from a pilocytic astrocytoma harboring *NF1* splice site and *PDGFRA* missense mutations. Postcontrast magnetic resonance imaging images show decrease in tumor size following 3 months of treatment with everolimus and trametinib.

Abbreviations: NF1, neurofibromatosis 1; PDGFRA, platelet derived growth factor receptor A.

GBM, alterations in *EGFR*, *PTEN*, *CDKN2A*, *and CDNK2B* were only observed in 7.8% (7/90), 15.6% (14/90), 20% (18/90), and 15.6% (14/90) of pediatric GBMs, respectively [23, 24]. However, *PDGFRA* alterations, including point mutations and amplifications, were observed in 25.6% (23/90) of cases, which is nearly twice the rate observed in adult GBMs (15%; Fig. 4A) [25].

Anaplastic astrocytomas showed frequent *EGFR* alterations (mutations and amplifications), *TP53* mutations, and *PIK3CA* mutations at rates of 40.7% (11/27), 33.3% (9/27), and 18.5% (5/27), respectively (Fig. 4B). Mutations in the *TERT* promoter were also frequent in AA3 tumors, with 25.9% (7/27) of tumors harboring the −124C>T variant. Four anaplastic astrocytomas (AAs) also harbored *H3F3A* K28M mutations that co-occurred

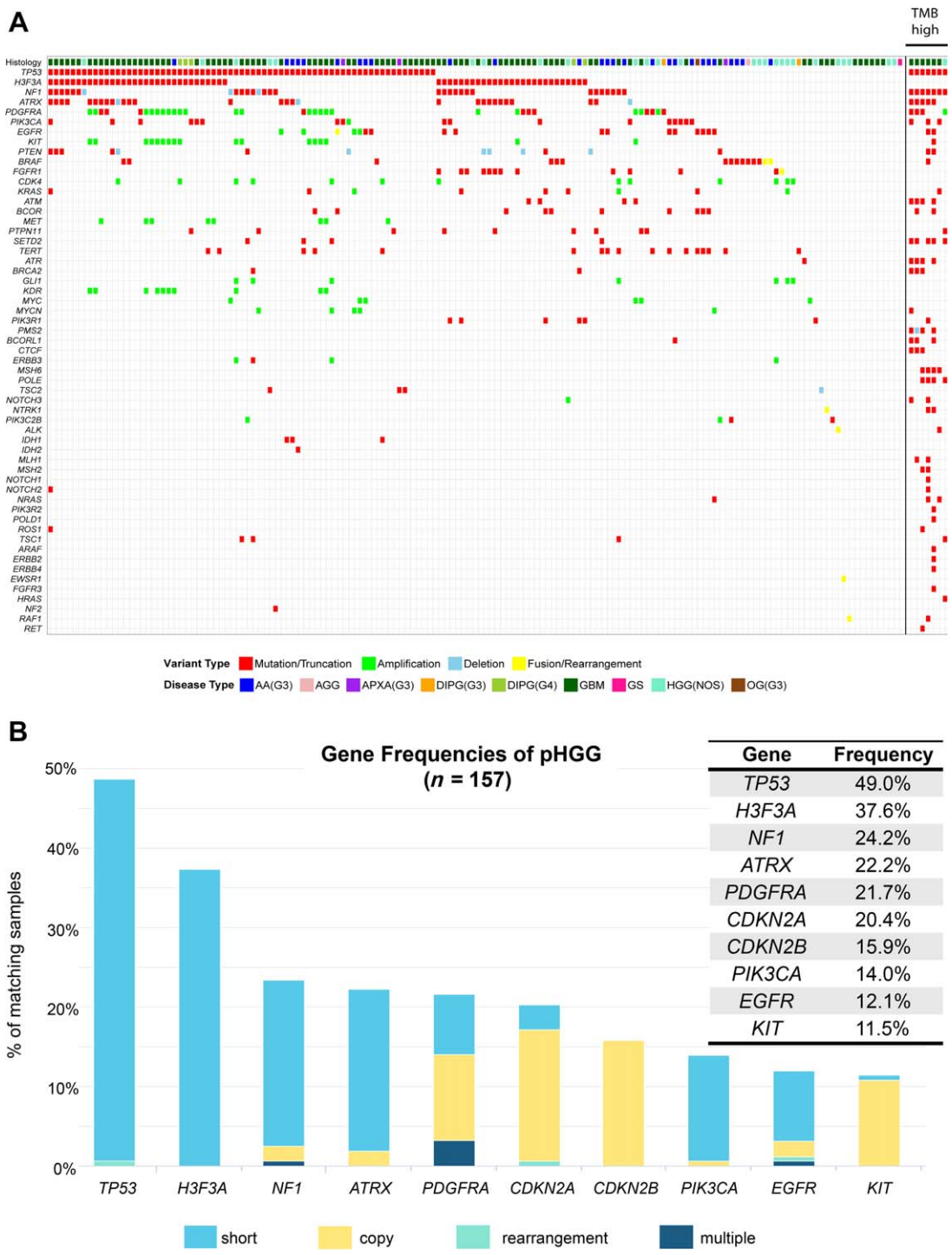

Figure 3. Genomic landscape of pHGG. **(A)**: Tile plot illustrating the type of recurrent genomic alterations ($n \geq 2$) and corresponding histologic diagnosis in 157 pHGGs. **(B)**: Long-tail distribution highlighting the top 10 altered genes in the pHGG cohort. Types of alterations are color-coded using key at bottom of bar graph.

Abbreviations: AA(G3), anaplastic astrocytoma grade III; AGG, anaplastic ganglioglioma; APXA, anaplastic pleomorphic xanthoastrocytoma grade III; G, grade; HGG, high-grade glioma; NOS, not otherwise specified; OG, oligodendroglial; pHGG, pediatric high-grade glioma.

with *PIK3R1*, *FGFR1* and *ATRX*, *PIK3CA* and *NF1*, or *TP53* mutations.

In the pHGG NOS cohort, *H3F3A* was altered in 23.1% (6/26) of cases, all of which were the K28M variant (Fig. 4C). *NF1* and *TP53* alterations were also frequent in pHGG NOS; they were detected in 23.1% (6/26) of tumors, co-occurring in five of the six cases. *NF1* alterations were predominately loss of function mutations (5/6 cases), with one tumor harboring a homozygous *NF1* deletion. *FGFR1* (19.2%, 5/26) and *PDGFRA* (19.2%, 5/26) alterations were also prevalent in pHGG NOS tumors. Three of five *FGFR1* mutated tumors harbored N546K variants co-occurring with other mutations including *CDKN2A/B* deletions, *PIK3CA* H1047R or *H3F3A* K28M mutations. Of the five PDGFRA altered tumors, four reported amplifications and

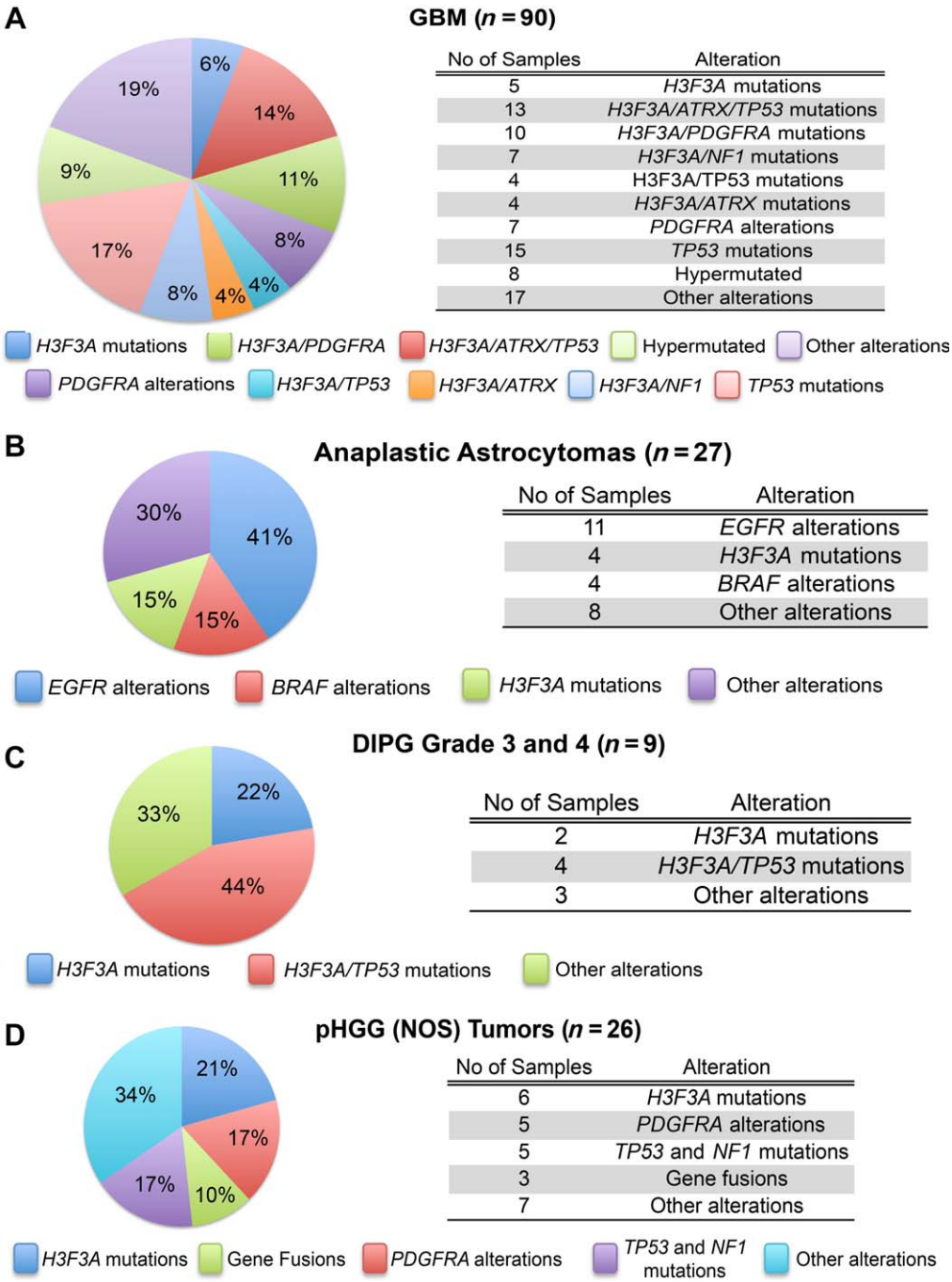

No of Samples	Alteration
5	*H3F3A* mutations
13	*H3F3A/ATRX/TP53* mutations
10	*H3F3A/PDGFRA* mutations
7	*H3F3A/NF1* mutations
4	H3F3A/TP53 mutations
4	*H3F3A/ATRX* mutations
7	*PDGFRA* alterations
15	*TP53* mutations
8	Hypermutated
17	Other alterations

No of Samples	Alteration
11	*EGFR* alterations
4	*H3F3A* mutations
4	*BRAF* alterations
8	Other alterations

No of Samples	Alteration
2	*H3F3A* mutations
4	*H3F3A/TP53* mutations
3	Other alterations

No of Samples	Alteration
6	*H3F3A* mutations
5	*PDGFRA* alterations
5	*TP53* and *NF1* mutations
3	Gene fusions
7	Other alterations

Figure 4. Distribution of commonly mutated genes and number of samples (table) harboring alterations in glioblastoma **(A)**, anaplastic astrocytomas **(B)**, DIPG (grade 3 and 4) **(C)**, and pHGG NOS tumors **(D)**.

Abbreviations: DIPG, diffuse intrinsic pontine glioma; EGFR, epidermal growth factor receptor; NOS, not otherwise specified; pHGG, pediatric high-grade glioma.

three of these tumors harbored co-occurring *CDKN2A/B* deletions (Fig. 4C).

Among high-grade DIPGs, *H3F3A* mutations were detected in 66.7% (6/9) of cases, with these cases reporting only the K28M variant (Fig. 4D). In the *H3F3A* mutated DIPGs, four harbored co-occurring *TP53* mutations and the other two tumors harbored *PTPN11* and *TERT* mutations or *CDKN2C* deletion and *PIK3R1* mutations. The three cases without *H3F3A* alterations reported only a *TERT* promoter −124C>T, *PDGFRA* D842del, or no reportable mutations, respectively.

The six anaplastic PXAs in our cohort reported a spectrum of mutations: one tumor harbored a *BRAF* V600E mutation with *CDKN2A/B* deletions and a *TERT* promoter mutation, whereas in the other PXAs, only *TP53* S183*, *PIK3CA* G118D, *TSC2* Y1033fs*1, *RB1* E672fs*5, or *RB1* T140fs*5 and *TP53* F109fs*14 mutations were detected.

Contrary to adult oligodendrogliomas, the one anaplastic oligodendroglioma in our cohort did not harbor *IDH1/2* mutations or 1p/19q co-deletion [19, 22, 26]. We detected *KRAS* G12V, *EGFR* R222C, and *TERT* promoter −124C>T mutations, a

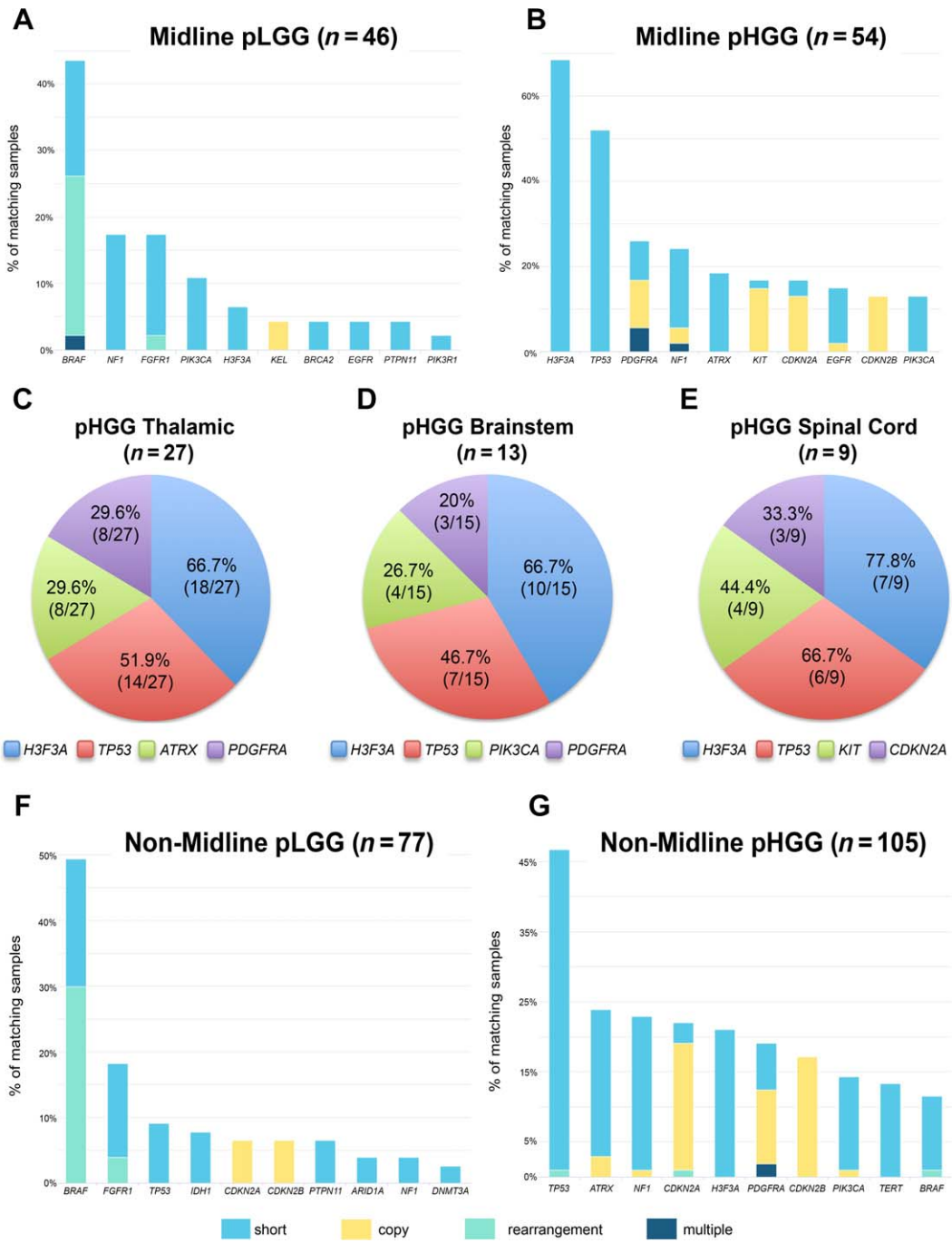

Figure 5. Long-tail distribution highlighting the top 10 altered genes in pLGG **(A)** and pHGG **(B)** midline tumors; distribution of most commonly mutated genes in pHGG thalamic **(C)**, brain stem **(D)**, and spinal cord **(E)** tumors. Long-tail distribution of the top 10 altered genes in pLGG **(F)** and pHGG **(G)** nonmidline tumors.

Abbreviations: EGFR, epidermal growth factor receptor; pHGG, pediatric high-grade glioma; pLGG, pediatric low-grade glioma.

genomic signature that better aligns with an astrocytic lineage glioma. Of the less prevalent histologic subtypes, one anaplastic ganglioglioma harbored a *BRAF* V600E mutation with a co-occurring *CDKN2A/B* deletion.

Genomic Analysis of Midline, Brainstem, and Spinal Cord Gliomas

The strongest clinical prognostic factors in pediatric gliomas include histologic grade and extent of resection, which is largely dependent on tumor location. We divided our cohort into midline and nonmidline tumors and examined the most frequently mutated genes in each group. Midline tumor locations included thalamus ($n = 37$), brainstem ($n = 31$), spinal cord ($n = 12$), hypothalamus ($n = 7$), basal ganglia ($n = 2$), and other (pineal, third and fourth ventricles; $n = 11$). Of the 282 samples, 35.5% ($n = 100$) were classified as midline, including 46 pLGGs and 54 pHGGs. The most common diagnoses among midline pLGGs were LGG NOS ($n = 17$), PA ($n = 16$), and DA2 ($n = 5$), and those among pHGGs were GBM ($n = 29$), AA3 ($n = 9$), DIPG ($n = 8$), and HGG NOS ($n = 8$).

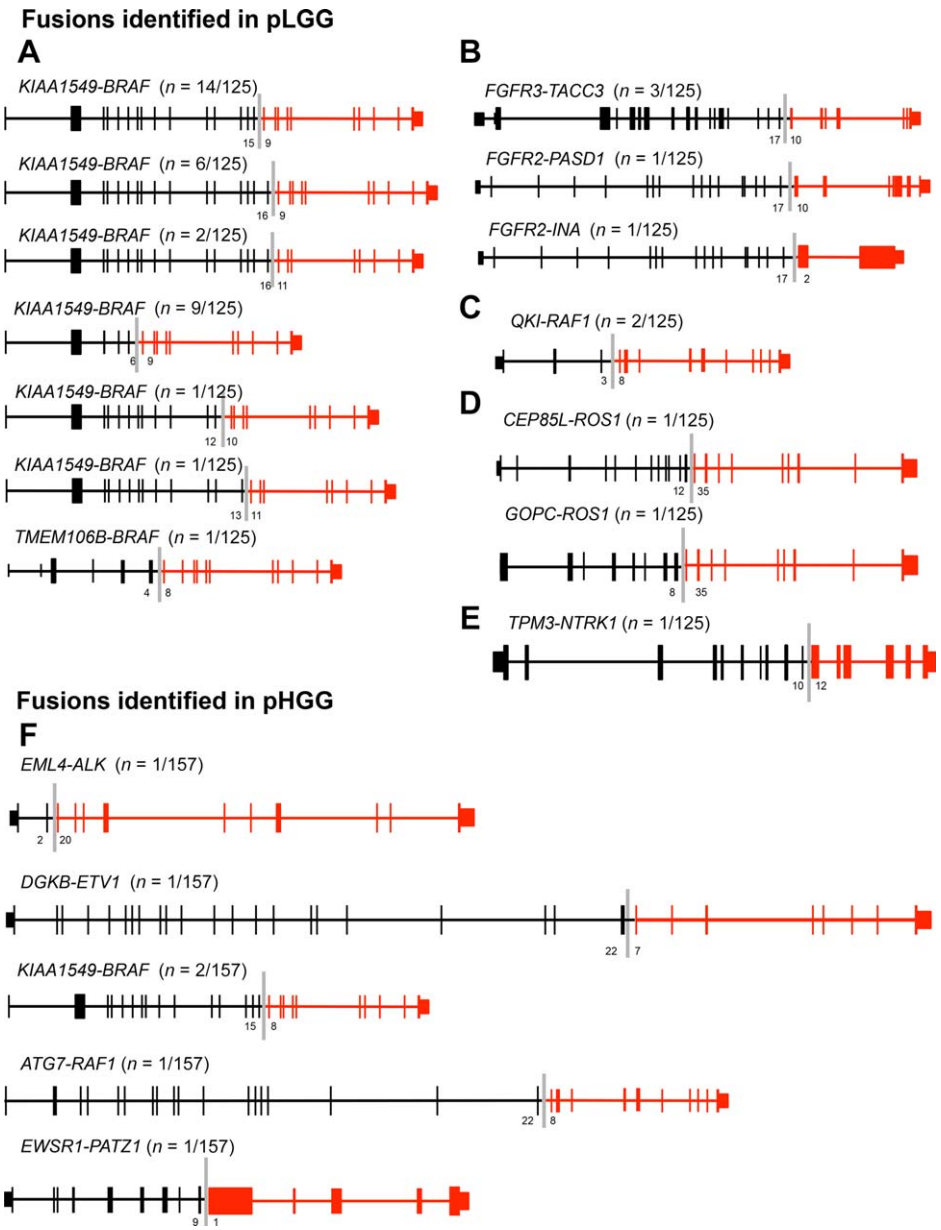

Figure 6. Schematics representing recurrent and novel kinase fusions identified in pLGGs **(A–E)** and pHGGs **(F)**; exon numbers at the fusion boundary are depicted below each diagram.

Abbreviations: pHGG, pediatric high-grade glioma; pLGG, pediatric low-grade glioma.

Overall, *H3F3A* was the most commonly altered gene in midline tumors, altered in 40% of cases, with the K28M variant detected in all 40 mutated cases (supplemental online Figure 2A). *TP53* mutations were detected in 28% (28/100) of cases, and among these, 20 harbored co-occurring *H3F3A* K28M mutations. Interestingly, *BRAF* alterations occurred in 25% (25/100) of midline gliomas, with 12 tumors harboring *KIAA1549-BRAF* fusions and 11 tumors with *BRAF* V600E mutations.

Among midline pLGGs, *BRAF* (43.5%), *NF1* (17.4%), *FGFR1* (17.4%), and *PIK3CA* (10.9%) were the most commonly altered genes (Fig. 5A). Among low-grade tumors, *H3F3A* was mutated in only 6.5% of cases. In contrast, the genes most commonly altered in midline pHGGs were *H3F3A* (68.5%), *TP53* (51.9%), *PDGRA* (25.9%), and *NF1* (24.1%; Fig. 5B). Among 27 thalamic pHGGs, *H3F3A* mutations were detected in 66.7% ($n = 18$) of tumors and entirely consisted of the K28M variant (Fig. 5C). Similarly, 66.7% (10/15) of high-grade brainstem gliomas and 77.8% (7/9) of spinal cord HGGs harbored *H3F3A* (K28M) mutations (Fig. 5D, 5E).

Of the 182 nonmidline gliomas, the most frequently mutated genes were *TP53* (30.8%, 56/182), *BRAF* (27.5%, 50/182), and *CDKN2A* (15.4%, 28/182; Fig. 5F, 5G, and supplemental online Fig. 2B). Twenty-four of the *BRAF*-altered nonmidline gliomas harbored fusions, 24 others had *BRAF* V600E mutations, and 2 tumors had *BRAF* S605G or D594G mutations. In nonmidline tumors, *H3F3A* mutations were detected in 12.1% (22/182) of cases, including 14 K28M and 8 G35R/V variants.

Gene Fusions Are Critical Driver Events in pLGGs and pHGGs

Gene fusions were most common among pLGGs, with 35.2% (44/125) of tumors harboring an in-frame fusion. Thirty-four of these fusions involved *BRAF*, and of these, 33 were *KIAA1549-*

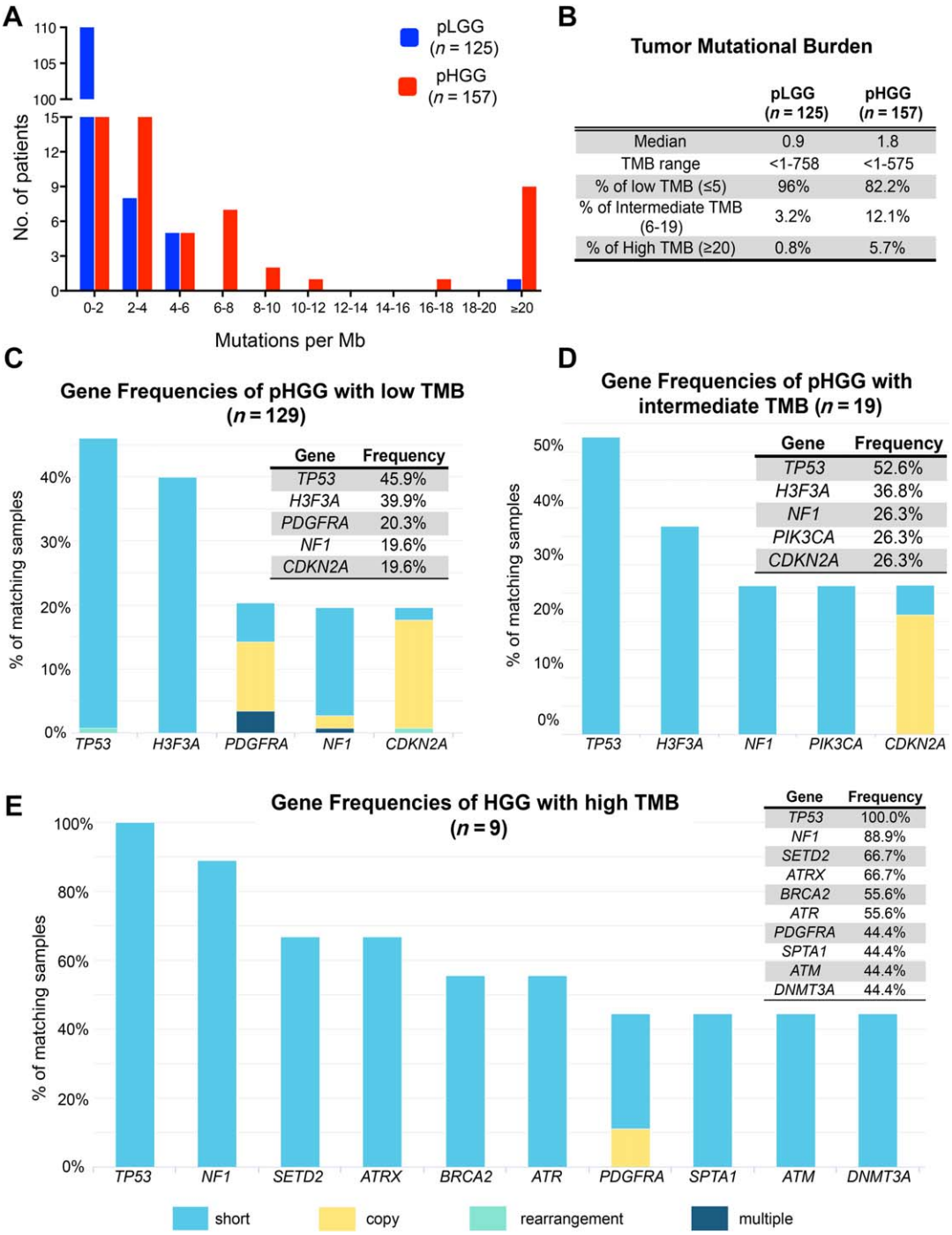

Figure 7. Tumor mutational burden in pHGGs and associated gene mutation frequencies. **(A)**: Distribution of tumor mutational burden in cohort of pLGG (blue) and pHGG (red). **(B)**: Summary of TMB statistics in pLGG and pHGG. Long tail distribution of the most commonly altered genes in pHGG with low **(C)**, intermediate **(D)**, and high **(E)** TMB.

Abbreviations: TMB, tumor mutational burden; HGG, high-grade glioma; Mb, megabase; pHGG, pediatric high-grade glioma; pLGG, pediatric low-grade glioma.

BRAF fusions. All the *KIAA1549-BRAF* fusions were in-frame and contained the *BRAF* kinase domain (Fig. 6A). Fourteen of these contained the first 15 exons of *KIAA1549* fused to exons 9–18 of *BRAF*, 6 involved the first 16 exons of *KIAA1549* fused to exons 9–18 of *BRAF*, 2 with exons 1–16 of *KIAA1549* fused to exons 11–18 of *BRAF*, 9 consisted of exons 1–6 of *KIAA1549* fused to exons 9–18 of *BRAF*, 1 consisted of exons 1–12 of *KIAA1549* fused to exons 10–18 of *BRAF*, and 1 contained exons 1–13 of *KIAA1549* fused to exons 11–18 of *BRAF*. The other *BRAF* fusion was detected in a GG and consisted of the first 4 exons of *TMEM106B* fused to exons 8–18 of *BRAF*. This fusion was also in-frame and contained the *BRAF* kinase domain. Three *FGFR3-TACC3* fusions were detected among pLGGs, including one diffuse astrocytoma, WHO grade II (DA), one oligodendroglioma, WHO Grade II (OG), and one pLGG NOS (Fig. 6B). All three of these fusions were in-frame, contained the *FGFR3* kinase domain, and consisted of the first 17 exons of *FGFR3* fused to exons 10–16 of *TACC3*. Two *FGFR2* in-frame

Table 1. Hypermutated pediatric GBMs harbor mutations in MMR pathway genes.

Sample ID	Age (years)	Sex	Diagnosis	Location	Newly diagnosed or recurrent	TMB	*MSH2*	*MSH6*	*MLH1*	*POLE*	*PMS2*	*POLD1*
1	14	M	GBM	Temporal	Recurrent	43	P622S	E484K, T1219I, G1218D, S998F	—	—	—	—
2	4	M	GBM	Frontal	Newly diagnosed	50	M485T, V63G	D439G, S1094P	—	—	K706fs*	I606M, R276M
3	13	M	GBM	Frontal	Recurrent	118	—	A159D, P105S, R243H, R988H	E34*	A1349V, M444K	two-copy loss exons 1-14, N45D	A288V
4	13	F	GBM	Frontal	Newly diagnosed	160	R406Q	R1035*, K476N, R1034W	—	L424I, V1270G	S46I, A520V	Q369H
5	15	F	GBM	Temporal	Recurrent	176	—	G1138E	—	A2180V	—	G705C
6	7	M	GBM	Temporal	Newly diagnosed	392	R406Q	R298*, 3647–6, 3647–1deltaacag, D268Y, S219I	R100*	S297F	—	—
7	7	F	GBM	Temporal	Recurrent	448	—	—	—	S461T, A1967V, P1432T, S780I	R315*	R652W, R689W
8	16	F	GBM	Spinal cord	Recurrent	581	T796N, V367I	R248fs*8, F115I, G1157C, P320S	Y245C	V411L, A288V, A789T	R421*, R169H	D635N, R211C, R689W
9	8	M	HGG (NOS)	Frontal	Newly diagnosed	95	K347E	R988H	E102D	E978G, F1366V, N251fs*12	—	T473M

Abbreviations: —, no data; F, female; GBM, glioblastoma; HGG, high-grade glioma; M, male; NOS, not otherwise specified; TMB, tumor mutational burden.

fusions that contained the kinase domain were also detected in the pLGG subgroup (Fig. 6B). The first was an *FGFR2-PASD1* fusion detected in an OG that consisted of exons 1–17 of *FGFR2* fused to exons 10–16 of *PASD1,* and the second was an *FGFR2-INA* fusion detected in a pLGG NOS that consisted of exons 1–17 of *FGFR2* fused to exons 2–3 of *INA*. Additionally, two in-frame *QKI-RAF1* fusions were detected in one OG and a recurrent PA (Fig. 6C). These fusions consisted of the first 3 exons of *QKI* fused to exons 8–17 of *RAF1*. We also identified *ROS1* fusions, including a *CEP85L-ROS1* detected in a recurrent DA2 and a *GOPC-ROS1* in a pLGG NOS. Although the fusion partner differed, both consisted of exons 35–43 of *ROS1* (Fig. 6D). Finally, a *TPM3-NTRK1* fusion was detected in a pLGG NOS that consisted of exons 1–10 of *TPM3* fused in-frame to exons 12–17 of *NTRK1*, which includes the *NTRK1* kinase domain (Fig. 6E).

Gene fusions were rare among pHGGs but were detected in six unique pHGG specimens (Fig. 6F). The first pHGG NOS harbored an in-frame *EML4-ALK* fusion, containing the first 2 exons of *EML4* fused to exons 20–29 of *ALK*. This variant, which has been previously described, comprises the components necessary and sufficient for cell transformation [27, 28]. In the second case, an in-frame *DGKB-ETV1* fusion was identified in a GBM and consisted of the first 22 *DGKB* exons fused to exons 7–14 of *ETV1*. In the two other cases, an in-frame *KIAA1549-BRAF* fusion was detected in a pHGG NOS and an AA3, wherein the first 15 exons of *KIAA1549* were fused to exons 9–18 of *BRAF* and included the kinase domain of *BRAF*. In a separate pHGG NOS, an *ATG7-RAF1* fusion was detected and consisted of exons 1–18 of *ATG* fused to exons 8–17 of *RAF1*. Lastly, an *EWSR1-PATZ1* fusion was identified in a pHGG NOS, which comprised exons 1–9 of *EWSR1* fused to exons 1–5 of *PATZ1*.

Hypermutant GBMs Enriched for Mutations in DNA Mismatch Repair Genes

Tumor mutational burden was calculated for all pLGGs and pHGGs and classified as low (0–<6), intermediate (6–20), or high (≥20). In pLGGs, TMBs ranged from <1 to 758, with a median of 0.9 mutations per Mb (Fig. 7A, 7B). All but one pLGG reported a low or intermediate TMB, with the single outlier harboring a TMB of 758 mutations per Mb, which was a recurrent cerebellar pLGG NOS in a late adolescent male.

In the pHGG group, the TMB ranged from <1 to 575, with a median of 1.8 mutations per Mb. The majority of tumors demonstrated a low TMB (82.2%, 129/157) compared with those in TMB-intermediate (12.1%, 19/157) and TMB-high groups (5.7%, 9/157; Fig. 7A, 7B). Although *TP53* mutations were the most frequent alteration across all pHGGs, *H3F3A* mutations were exclusive to tumors with low and intermediate TMBs (Fig. 7C, 7D). The average TMB of *H3F3A* mutated pHGGs was 1.8 mutations per Mb and ranged from <1 to 17.1, highlighting that these mutations are mutually exclusive from hypermutated pHGGs in our dataset. The remaining 6% (9/157) of pHGGs were classified as hypermutated, with TMBs ranging from 43–575 mutations per Mb, and all harbored mutations in *TP53* (100%, 9/9), *NF1* (88.9%, 8/9), *SETD2* (66.7%, 6/9), and *ATRX* (66.7%, 6/9; Fig. 7E). Such high mutation rates raised the possibility of biallelic mismatch repair disease (bMMRD). Among the nine pHGGs (four newly diagnosed, five recurrent) with a high TMB, six harbored functional mutations in mismatch repair (MMR) or proofreading genes *MSH2, MSH6, MLH1, POLE, PMS2*, or *POLD1* (Table 1), whereas the other three tumors harbored variants of

unknown significance in these MMR genes. Interestingly, functional mutations in bMMRD genes were not detected in pHGG tumors with low or intermediate TMB.

Discussion

In this study, 282 pediatric gliomas were analyzed by CGP and genomic alterations were identified in over 95% of cases. Among pLGGs, the most common alterations were *BRAF* alterations, followed by *FGFR1* lesions, whereas in pHGGs, *TP53* and *H3F3A* mutations dominated the genomic landscape. Surprisingly, in our pHGG cohort, the *H3F3A* K28M variant ($n = 51$) was most prevalent, with only 8 of 59 pGBM cases with *H3F3A* mutations reporting a G35R variant; midline tumors also enriched for K28M variant. Additionally, only the K28M variant was detected in pLGGs harboring *H3F3A* mutations. The presence of *H3F3A* mutations in pLGGs has significant clinical impact because previous reports demonstrated that the prognosis for K28M mutated gliomas is worse compared with G34R and wild-type *H3F3A* cases [10, 21, 22].

We also identified recurrent and novel fusions in both pLGGs and pHGGs. We report *EML4-ALK*, *DGKB-ETV1, KIAA1549-BRAF, ATG7-RAF1*, and *EWSR1-PATZ1* rearrangements in pHGGs. Because these fusions have been previously reported, we hypothesize that they are the main oncogenic drivers. Furthermore, these patients may benefit from currently available small molecule inhibitors that disrupt the oncogenic fusion activity, as is the case for *EML4-ALK* fusions in NSCLCs, which respond to the ALK inhibitors [29].

Although surgical resection remains the most effective treatment option for pLGGs, tumors located in eloquent areas not amenable to surgical resection (e.g., motor cortex) require alternative therapeutic strategies. Recent reports highlight tumor regression of *BRAF* mutated pLGGs in response to dabrafenib, a BRAF inhibitor, and several clinical trials of BRAF inhibitors are ongoing for pediatric patients with *BRAF*-mutated gliomas [30]. Furthermore, a clinical trial (NCT01734512) open for recurrent pLGGs aims to evaluate the efficacy of everolimus, an mTOR inhibitor. We report a multiply recurrent *NF1* mutated PA previously treated with surgery alone that now shows a remarkable response to dual inhibitor therapy (everolimus and trametinib) following 3 months of treatment. Ongoing *H3F3A* K28M peptide vaccine trials (NCT02960230) represent another active area of investigation for DIPG patients.

Conclusion

With increasing reports of high TMB in gliomas, immunotherapy has emerged as a novel therapeutic strategy for adult and pediatric brain tumors. More recently, interrogation of sequencing data has revealed TMB as a critical biomarker for predicting responses to therapy [31, 32]. In the adult population, hypermutated or TMB-high cancers have been reported to respond to immune checkpoint inhibitors (ICPI) [33]. As previously reported, bMMRD pediatric glioma patients experienced durable responses to ICPI at tumor recurrence following standard of care [11]. We identified nine patients with hypermutated gliomas characterized by TMBs ranging from 43 to 575 mutations per Mb, and representing a genomically distinct group of pHGGs. Given that these patients may preferentially benefit from ICPI, these findings demonstrate how CGP can reliably and routinely identify hypermutated gliomas.

Acknowledgments

This study was supported by Foundation Medicine, Inc.

Author Contributions

Conception/design: Adrienne Johnson, Eric Severson, Siraj Ali, John Crawford, Shakti Ramkissoon
Financial support: N/A
Administrative support: N/A
Provision of study material or patients: John Crawford
Collection and/or assembly of data: Adrienne Johnson, Eric Severson, Laurie Gay, Mandy Covert, Garrett Frampton, Sigmund Hsu, Glenn J. Lesser, Kimberly Stogner-Underwood, Ryan T. Mott, Sarah Z. Rush, Jennifer J. Stanke, Sonika Dahiya, James Sun, Prasanth Reddy, John Crawford, Shakti Ramkissoon
Data analysis and interpretation: Adrienne Johnson, Eric Severson, Laurie Gay, Mandy Covert, Garrett Frampton, Zach Chalmers, Rachel Erlich, Yakov Chudnovsky, David Fabrizio, Alexa B. Schrock, Siraj Ali, John Crawford, Shakti Ramkissoon
Manuscript writing: Adrienne Johnson, Eric Severson, Laurie Gay, Mandy Covert, Siraj Ali, John R. Crawford, Shakti H. Ramkissoon
Final approval of manuscript: Adrienne Johnson, Eric Severson, Laurie Gay, Jo-Anne Vergilio, Julia Elvin, James Suh, Sugganth Daniel, Mandy Covert, Garrett M. Frampton, Sigmund Hsu, Glenn J. Lesser, Kimberly Stogner-Underwood, Ryan T. Mott, Sarah Z. Rush, Jennifer J. Stanke, Sonika Dahiya, James Sun, Prasanth Reddy, Zachary R. Chalmers, Rachel Erlich, Yakov Chudnovsky, David Fabrizio, Alexa B. Schrock, Siraj Ali, Vincent Miller, Philip J. Stephens, Jeffrey Ross, John R. Crawford, Shakti H. Ramkissoon

Disclosures

Adrienne Johnson: Foundation Medicine, Inc. (E, OI); **Eric Severson**: Foundation Medicine, Inc. (E, OI); **Laurie Gay**: Foundation Medicine, Inc. (E, OI); **Jo-Anne Vergilio**: Foundation Medicine, Inc. (E, OI); **Julia Elvin**: Foundation Medicine, Inc. (E, OI); **James Suh**: Foundation Medicine, Inc. (E, OI); **Sugganth Daniel**: Foundation Medicine, Inc. (E, OI); **Mandy Covert**: Foundation Medicine, Inc. (E, OI); **Garret M. Frampton**: Foundation Medicine, Inc. (E, OI); **Sigmund Hsu**: AbbVie, Cortice Pharmaceutical (RF), Foundation Medicine, Inc. (H); **Glenn J. Lesser**: Insys Therapeutics (C/A), Incyte, New Link Genetics, Novartis, Pfizer, Vascular Biogenics (RF), Stemline Therapeutics (SAB); **James Sun**: Foundation Medicine, Inc. (E, OI); **Prasanth Reddy**: Foundation Medicine, Inc. (E, OI); **Zach Chalmers**: Foundation Medicine, Inc. (C/A, E, OI); **Rachel Erlich**: Foundation Medicine, Inc. (E, OI); **Yakov Chudnovsky**: Foundation Medicine, Inc. (E, OI); **David Fabrizio**: Foundation Medicine, Inc. (E, OI); **Alexa B. Schrock**: Foundation Medicine, Inc. (E, OI); **Siraj Ali**: Foundation Medicine, Inc. (E, IP, OI); **Vincent Miller**: Foundation Medicine, Inc. (E, OI); **Philip J. Stephens**: Foundation Medicine (E, OI); **Jeffrey Ross**: Foundation Medicine, Inc. (E, RF, OI); **Shakti H. Ramkissoon**: Foundation Medicine, Inc. (E, OI). The other authors indicated no financial relationships.

(C/A) Consulting/advisory relationship; (RF) Research funding; (E) Employment; (ET) Expert testimony; (H) Honoraria received; (OI) Ownership interests; (IP) Intellectual property rights/inventor/patent holder; (SAB) Scientific advisory board

References

1. Pui CH, Gajjar AJ, Kane JR et al. Challenging issues in pediatric oncology. Nat Rev Clin Oncol 2011;8:540–549.

2. Pfister S, Janzarik WG, Remke M et al. BRAF gene duplication constitutes a mechanism of MAPK pathway activation in low-grade astrocytomas. J Clin Invest 2008;118:1739–1749.

3. Dias-Santagata D, Lam Q, Vernovsky K et al. BRAF V600E mutations are common in pleomorphic xanthoastrocytoma: Diagnostic and therapeutic implications. PLoS One 2011;6:e17948.

4. Jones DT, Kocialkowski S, Liu L et al. Tandem duplication producing a novel oncogenic braf fusion gene defines the majority of pilocytic astrocytomas. Cancer Res 2008;68:8673–8677.

5. Dougherty MJ, Santi M, Brose MS et al. Activating mutations in BRAF characterize a spectrum of pediatric low-grade gliomas. Neuro Oncol 2010;12:621–630.

6. Bandopadhayay P, Ramkissoon LA, Jain P et al. MYB-QKI rearrangements in angiocentric glioma

drive tumorigenicity through a tripartite mechanism. Nat Genet 2016;48:273–282.

7. Zhang J, Wu G, Miller CP et al. Whole-genome sequencing identifies genetic alterations in pediatric low-grade gliomas. Nat Genet 2013;45:602–612.

8. Khuong-Quang DA, Buczkowicz P, Rakopoulos P et al. K27M mutation in histone H3.3 defines clinically and biologically distinct subgroups of pediatric diffuse intrinsic pontine gliomas. Acta Neuropathol 2012;124:439–447.

9. Schwartzentruber J, Korshunov A, Liu XY et al. Driver mutations in histone H3.3 and chromatin remodelling genes in paediatric glioblastoma. Nature 2012;482:226–231.

10. Sturm D, Witt H, Hovestadt V et al. Hotspot mutations in H3F3A and IDH1 define distinct epigenetic and biological subgroups of glioblastoma. Cancer Cell 2012;22:425–437.

11. Bouffet E, Larouche V, Campbell BB et al. Immune checkpoint inhibition for hypermutant glioblastoma multiforme resulting from germline biallelic mismatch repair deficiency. J Clin Oncol 2016; 34:2206–2211.

12. Bloch O, Crane CA, Kaur R et al. Gliomas promote immunosuppression through induction of B7-H1 expression in tumor-associated macrophages. Clin Cancer Res 2013;19:3165–3175.

13. Preusser M, Berghoff AS, Wick W et al. Clinical neuropathology mini-review 6-2015: PD-L1: Emerging biomarker in glioblastoma? Clin Neuropathol 2015;34:313–321.

14. Martin-Liberal J, Ochoa de Olza M, Hierro C et al. The expanding role of immunotherapy. Cancer Treat Rev 2017;54:74–86.

15. Scheel AH, Ansen S, Schultheis AM et al. PD-L1 expression in non-small cell lung cancer: Correlations with genetic alterations. Oncoimmunology 2016;5: e1131379.

16. Gibney GT, Weiner LM, Atkins MB. Predictive biomarkers for checkpoint inhibitor-based immunotherapy. Lancet Oncol 2016;17:e542–e551.

17. Johanns TM, Miller CA, Dorward IG et al. Immunogenomics of hypermutated glioblastoma: A patient with germline pole deficiency treated with checkpoint blockade immunotherapy. Cancer Discov 2016;6:1230–1236.

18. Bamford S, Dawson E, Forbes S et al. The COSMIC (Catalogue of Somatic Mutations in Cancer) database and website. Br J Cancer 2004;91:355–358.

19. Cryan JB, Haidar S, Ramkissoon LA et al. Clinical multiplexed exome sequencing distinguishes adult oligodendroglial neoplasms from astrocytic and mixed lineage gliomas. Oncotarget 2014;5:8083–8092.

20. Cancer Genome Atlas Research Network, Brat DJ, Verhaak RG et al. Comprehensive, integrative genomic analysis of diffuse lower-grade gliomas. N Engl J Med 2015;372:2481–2498.

21. Korshunov A, Ryzhova M, Hovestadt V et al. Integrated analysis of pediatric glioblastoma reveals a subset of biologically favorable tumors with associated molecular prognostic markers. Acta Neuropathol 2015;129:669–678.

22. Ryall S, Krishnatry R, Arnoldo A et al. Targeted detection of genetic alterations reveal the prognostic impact of H3K27M and MAPK pathway aberrations in paediatric thalamic glioma. Acta Neuropathol Commun 2016;4:93.

23. Gao J, Aksoy BA, Dogrusoz U et al. Integrative analysis of complex cancer genomics and clinical profiles using the cBioPortal. Sci Signal 2013; 6:pl1.

24. Cerami E, Gao J, Dogrusoz U et al. The cBio cancer genomics portal: An open platform for exploring multidimensional cancer genomics data. Cancer Discov 2012;2:401–404.

25. Cancer Genome Atlas Research Network. Comprehensive genomic characterization defines human glioblastoma genes and core pathways. Nature 2008;455:1061–1068.

26. Ramkissoon SH, Bi WL, Schumacher SE et al. Clinical implementation of integrated whole-genome copy number and mutation profiling for glioblastoma. Neuro Oncol 2015;17:1344–1355.

27. Inamura K, Takeuchi K, Togashi Y et al. EML4-ALK fusion is linked to histological characteristics in a subset of lung cancers. J Thorac Oncol 2008;3:13–17.

28. Choi YL, Takeuchi K, Soda M et al. Identification of novel isoforms of the EML4-ALK transforming gene in non-small cell lung cancer. Cancer Res 2008; 68:4971–4976.

29. Gerber DE, Minna JD. ALK inhibition for non-small cell lung cancer: From discovery to therapy in record time. Cancer Cell 2010;18:548–551.

30. Robinson GW, Orr BA, Gajjar A. Complete clinical regression of a BRAF V600E-mutant pediatric glioblastoma multiforme after BRAF inhibitor therapy. BMC Cancer 2014;14:258.

31. Topalian SL, Taube JM, Anders RA et al. Mechanism-driven biomarkers to guide immune checkpoint blockade in cancer therapy. Nat Rev Cancer 2016;16:275–287.

32. Rizvi NA, Hellmann MD, Snyder A et al. Cancer immunology. Mutational landscape determines sensitivity to PD-1 blockade in non-small cell lung cancer. Science 2015;348:124–128.

33. Postow MA, Callahan MK, Wolchok JD. Immune checkpoint blockade in cancer therapy. J Clin Oncol 2015;33:1974–1982.

See http://www.TheOncologist.com for supplemental material available online.